

Article

Improving the Corrosion Resistance of AZ91 Magnesium Alloy by Surface Coating TiO₂ Layers

Diqing Wan *, Hao Tang, Yumeng Sun, Guilin Zeng, Shaoyun Dong, Guoliang Han, Yu Wang, Fan Yang and Yongyong Wang

School of Materials Science and Engineering, East China Jiaotong University, Nanchang 330000, China; tanghao1020@163.com (H.T.); 13057107250@163.com (Y.S.); 18797974514@163.com (G.Z.); dsydongshaoyun@163.com (S.D.); h1314065009@163.com (G.H.); w1253830356@163.com (Y.W.); yf168898@163.com (F.Y.); wyy123456acb@163.com (Y.W.)

* Correspondence: divadwan@163.com

Abstract: This study adopts the sol-gel method to prepare a TiO₂ coating on the surface of the AZ91 magnesium alloy, hydrolyse C₁₆H₃₆O₄Ti to generate the TiO₂ coating and form a film with excellent corrosion resistance on the surface of an AZ91 magnesium alloy. The composition, surface structure and microstructure of the TiO₂ coatings are characterised via X-ray diffraction (XRD) and scanning electron microscopy. The corrosion performance of the surface coatings was investigated through hydrogen evolution experiments and electrochemical tests. The results demonstrate that TiO₂ sols prepared from a mixture of hydrochloric acid, deionised water, C₁₆H₃₆O₄Ti and anhydrous ethanol can form stable layers on the surface of an AZ91 magnesium alloy after heat treatment. The results of hydrogen evolution experiments and electrochemical tests reveal that the TiO₂ coating can effectively improve the corrosion resistance of the AZ91 magnesium alloy.

Keywords: AZ91 magnesium alloy; coating design; TiO₂ film; corrosion resistance



Citation: Wan, D.; Tang, H.; Sun, Y.; Zeng, G.; Dong, S.; Han, G.; Wang, Y.; Yang, F.; Wang, Y. Improving the Corrosion Resistance of AZ91 Magnesium Alloy by Surface Coating TiO₂ Layers. *Metals* **2023**, *13*, 1400. <https://doi.org/10.3390/met13081400>

Academic Editor: Petros E. Tsakiridis

Received: 13 July 2023

Revised: 1 August 2023

Accepted: 3 August 2023

Published: 5 August 2023



Copyright: © 2023 by the authors. Licensee MDPI, Basel, Switzerland. This article is an open access article distributed under the terms and conditions of the Creative Commons Attribution (CC BY) license (<https://creativecommons.org/licenses/by/4.0/>).

1. Introduction

Magnesium alloys have been hailed as the green engineering material of the 21st century for their low density, high strength, good damping and shock absorption, and greater ability to withstand impact loads than other alloys [1]. The majority of magnesium alloys generally have densities between 1.75 and 1.90 g/cm³, which is roughly 80% less dense than steel, 60% less dense than titanium, and 40% less dense than aluminium alloys. In addition to low density, magnesium alloy has many other excellent properties, such as good plasticity, high specific strength and specific modulus, good low-temperature toughness, insensitivity to notching, anisotropy is not obvious, etc. The magnesium alloys are the lightest of the practical metals and have the advantages of high specific strength and stiffness, damping and vibration and noise reduction as well as excellent electromagnetic shielding and easy machining and recycling. In recent years, magnesium alloys have been widely used in the aerospace, transportation, electronics, chemical and metallurgical industries.

Magnesium alloys are very easily corroded in wet environments, which has limited the development and wider application of magnesium alloys. Hence, improving the corrosion resistance of magnesium alloys is a hot topic [2–6].

Two main methods of improving the corrosion resistance of magnesium alloys exist. One is improving the intrinsic corrosion resistance of magnesium alloys, that is, by optimising the alloy composition and improving the microstructure of magnesium alloys to improve the corrosion resistance of the material [7]. The second is protecting the matrix using a surface protection layer to isolate the corrosive medium from the matrix [8]. One of the relatively effective and easy ways to improve the corrosion resistance of magnesium alloys is to make the surface of alloys treated. The aim of this study is to prepare a TiO₂

film on the surface of magnesium alloys, thereby improving the corrosion resistance of the surface of magnesium alloys. The so-called preparation of titanium dioxide film is titanium dioxide or titanium dioxide precursors coated on the substrate, so as to form a layer of titanium dioxide film on the surface of the substrate; therefore, this can be regarded as a coating process. The preparation of the TiO₂ film can encompass a variety of methods, the simplest of which is to obtain the TiO₂ nanoparticle coating (smear) (drop-coating, spin-coating, throwing film, spraying, pulling film, etc.) on the substrate after drying and baking. The key to this method is the preparation of TiO₂ nanoparticle colloids. The sol-gel method is the most commonly used means of preparing nanoparticles. The technique has the advantages of high purity, high homogeneity, low synthesis temperature and the easy control of reaction conditions, especially since the preparation process is relatively simple and does not require special expensive instruments, showing broad application prospects in the preparation of thin films, ultra-fine powders, composite functional materials, fibres and high melting point glasses and is the most commonly used method for preparing nanoparticles such as TiO₂, ZnO, WO₃, SnO₂, Fe₂O₃, Al₂O₃, etc. [9–11]. The sol-gel method has many advantages and is currently the ideal technique for the preparation of thin film coatings on magnesium alloys. In this paper, to improve the corrosion resistance of the AZ91 magnesium alloys, different thicknesses of TiO₂ coatings were prepared on the surface of such an alloy, using the sol-gel method [12], and the corrosion resistance was investigated through hydrogen evolution experiments and electrochemical tests and the composition and microstructure of the surface coatings were observed using an XRD diffractometer and a scanning electron microscope (SEM) [13].

2. Experiments and Methods

The chemical reagents needed for the experiment included acetone solution, C₁₆H₃₆O₄Ti solution, deionised water, hydrochloric acid and anhydrous ethanol. Acetone solution clears the sample surface and removes oil stains, C₁₆H₃₆O₄Ti solution supplies Ti for preparing TiO₂ nanopowder and hydrochloric acid and deionised water serve as stabilisers to slow the hydrolysis reaction rate of C₁₆H₃₆O₄Ti. In this paper, some of the main instruments and equipment used were a cutting machine (for cutting samples, Jincheng CNC Technology Taizhou Co., Ltd., Taizhou, China), metallographic sample polishing machine (Shanghai Reedon Instrumentation & Testing Technology Co., Shanghai, China), cased resistance-heated furnace (for heat treatment, Shanghai Pudong Rongfeng Scientific Instrument Co., Shanghai, China), X-ray diffractometer (XRD, Shimadzu Corporation, Kyoto, Japan) and scanning electron microscope (SEM, Hitachi High-Technologies Corporation, Shenzhen, China). The instrument used for the hydrogen evolution test included a dropper, butterfly clip, measuring cup and 3.5% NaCl solution. Electrochemistry was performed via a CHI660e electrochemical workstation (Shanghai Chenhua Instrument Co., Shanghai, China). The electrochemical measurement parameters are as follows: open-circuit potential test time was 300 s, sampling interval was 0.1 s; the frequency range of the EIS test was 1–10⁵ Hz; the amplitude was 0.01 V; the starting potential in the Tafel test was −1.8~(−0.8)V; and the scan rate was 0.01 V/s.

C₁₆H₃₆O₄Ti solution (5 mL) and anhydrous ethanol (20 mL) were mixed and stirred evenly and placed in a magnetic stirrer for continuous stirring. Under stirring, a mixed solution of 5 mL deionised water and 1 mL of hydrochloric acid were slowly and evenly dropped into the mixed solution of C₁₆H₃₆O₄Ti and anhydrous ethanol, and high-speed stirring was maintained for 2 h without generating flocculent precipitation. Finally, a light-yellow transparent solution was obtained. The solution was allowed to stand for 24 h to prepare the subsequent alloy surface coating [14]. The AZ91 magnesium alloy was cut into small 15 mm × 15 mm squares 5 mm thick using a wire cutter. It was then sanded with 400–7000 grit sandpaper and polished with a metallographic grinding and polishing machine to achieve a smooth surface. The specimens were then soaked in acetone solution for 1–2 min and were cleaned via ultrasonic shaking to remove the oil, blown dry, and set aside.

The specimen was immersed into the above prepared solution using the lifting method, so that came into full contact with the solution, and its surface was fully covered with a layer of TiO₂ film, then it was placed in thermostat at 300 °C for 2 h to be heat treated in order to obtain the AZ91 magnesium alloy specimen coated with one layer of TiO₂ (here after referred to as sample 1). Using the same method, after coating once with the sol, the sample was placed into the thermostat at 100 °C for 0.5 h, then the next layer of sample was coated, and this step was repeated 3 times. Finally, the sample was placed in a thermostat at 300 °C for 2 h to obtain AZ91 magnesium alloy specimens coated with 3 layers of TiO₂ (here after referred to as sample 2). After coating once with the sol, the sample was placed in a thermostat and was dried at 100 °C for 0.5 h, then the next layer was continued to be coated, and this step was repeated 5 times. The sample was then placed in a thermostat at 300 °C for 2 h to be heat treated. Thus a sample of an AZ91 magnesium alloy coated with 5 layers of TiO₂ was obtained (here after referred to as sample 3) [15]. The process parameters are shown in Table 1. Surface composition analysis and microstructure observation of the produced AZ91 matrix, sample 1, sample 2 and sample 3 were performed using an XRD diffractometer and SEM. The corrosion properties of the AZ91 matrix, sample 1, sample 2 and sample 3 were determined via hydrogen evolution experiments and electrochemical tests using a 3.5% NaCl solution [16,17]. The measurement parameter of the hydrogen evolution test was the amount of hydrogen released from the sample after 12 h of corrosion in a 3.5% NaCl solution (the less the hydrogen evolution, the better the corrosion resistance of the alloy).

Table 1. Process parameters of AZ91 matrix and sample layers.

Specimen Designation	Coating Numbers	Parameter of Heat Treatment				
		Drying Temperature (°C)	Drying Time (h)	Drying Times (h)	Holding Temperature (°C)	Holding Time (h)
AZ91 matrix	-	-	-	-	-	-
Sample 1	1	-	-	-	300	2
Sample 2	3	100	0.5	2	300	2
Sample 3	5	100	0.5	4	300	2

3. Results and Discussion

3.1. Microstructure of TiO₂-Coated AZ91 Magnesium Alloy

The three different types of TiO₂ are rutile, anatase, and platinoid, with anatase being the most active and rutile being the most inactive. The anatase crystalline form of TiO₂ is substable and transforms into rutile crystalline form at high temperatures [18]. The XRD test results of the anatase TiO₂ coating before and after heat treatment at 300 °C are shown in Figure 1.

Figure 1 shows XRD patterns of samples. The peaks of anatase TiO₂ were observed for samples 1, 2 and 3. This information along with the 2θ angle of the characteristic peak and the spatial point group of TiO₂ in the related literature indicates that the coating provided was anatase TiO₂. The analysis suggested that during the preparation of the sol, C₁₆H₃₆O₄Ti provided the metal element, which underwent a hydrolysis and condensation reaction with water, and a small amount of hydrochloric acid controlled the rate of the hydrolysis reaction, which yielded TiO₂. TiO₂ powder was obtained by heating the sols coated on the sample surface for 30 min at 100 °C, and it was then deposited on the AZ91 surface through a 2 h heat treatment process performed at 300 °C to provide a TiO₂ coating.

The results of the SEM analysis of alloy surface coatings are shown in Figure 2. Figure 2a shows that the surface of the AZ91 matrix was mostly flat and smooth, with a regular and ordered microstructure and many tiny voids. In Figure 2b, the TiO₂ coating of sample 1 can be observed to have small cracks, with the AZ91 matrix being exposed at the crack seam, and the coating layer is missing in some areas. Although the coverage of the AZ91 matrix is good, the small thickness of the layer and the presence of cracks render the coating insufficient for the protection of AZ91. In Figure 2c, it can be seen

that the thickness of the TiO₂ coating of sample 2 increased significantly on the basis of sample 1 (one layer). The outermost layer had a large number of fractured areas but was deposited on top of a more complete and well-bonded substrate coating. The TiO₂ coating material had accumulated in some areas, and together with the increased coating thickness, it improved the protection of the matrix. In Figure 2d, compared with sample 2, the coating thickness of sample 3 is larger, and the coating is denser and finer, with the outermost layer of the coating being significantly less fragmented. Furthermore, the accumulation of the TiO₂ coating material in sample 3 was comparatively greater, and the coating took the form of fine flakes; only a small part of the thickness did not increase, revealing the substrate coating.

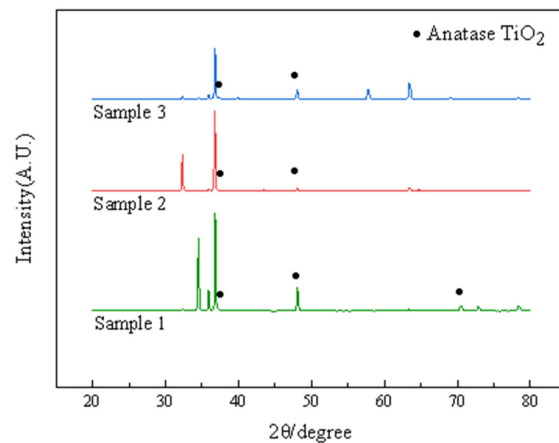


Figure 1. XRD patterns of AZ91 magnesium alloys coated by TiO₂.

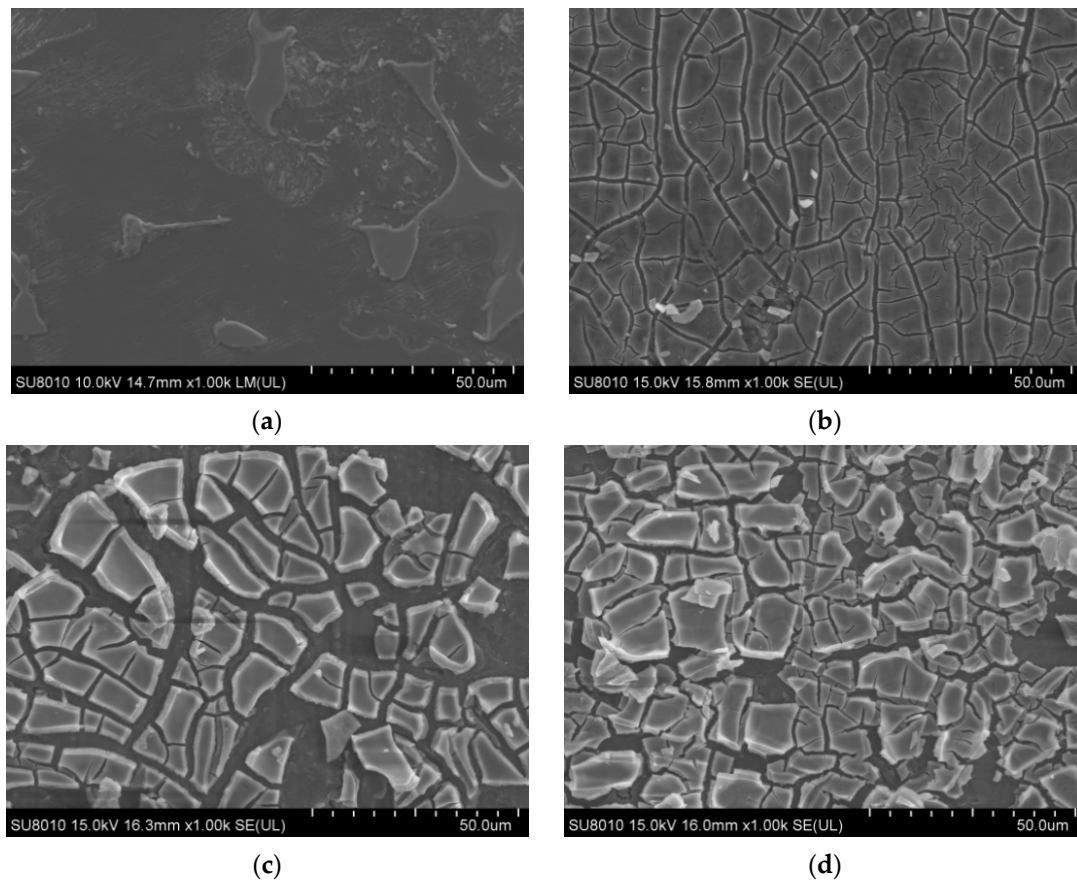


Figure 2. Microstructure of the alloy surface coating with different number of coats (a) AZ91 matrix; (b) sample 1; (c) sample 2; (d) sample 3.

The specimen was immersed in the sol by using the lifting method. The surface of the AZ91 magnesium alloy was covered with a sol-gel film whose thickness was greater than the ideal thickness, and this resulted in the curing rates of the surface and bottom layers of the sol-gel film being different. The surface layer cured faster, and the top layer was cracked when the solvent of the bottom layer evaporated outward. The TiO₂ film became brittle and cracked during the heating process, and the crack could be observed in the microscopic morphology of the TiO₂ coating of sample 1. After the sol film on the surface of the AZ91 substrate was heated at 100 °C for 30 min to produce TiO₂ powder, the substrate was again coated with a TiO₂ film by using the lifting method. For samples 3 and 5, multilayer coating was provided on a pre-existing single layer of TiO₂ coating [19]. Unlike its adhesion to the substrate surface, TiO₂ did not adhere firmly to the bottom coating, and thus, the theoretical number of coatings on samples 3 and 5 fell short of providing the ideal protection level required. Overall, the protection of the matrix alloy had improved.

3.2. Corrosion Resistance of TiO₂-Coated AZ91 Magnesium Alloy Surface

Figure 3 shows that the amount of hydrogen evolution in the NaCl solution within 12 h was reduced by 54.3%, 71.8% and 74.2% for samples 1, 2 and 3 compared with the AZ91 matrix, respectively. In particular, the amount of hydrogen evolution was the smallest for sample 3. This shows that a TiO₂ coating can effectively reduce the amount of hydrogen evolution for the AZ91 matrix immersed in NaCl solution and thereby enhance the corrosion resistance of the AZ91 matrix surface.

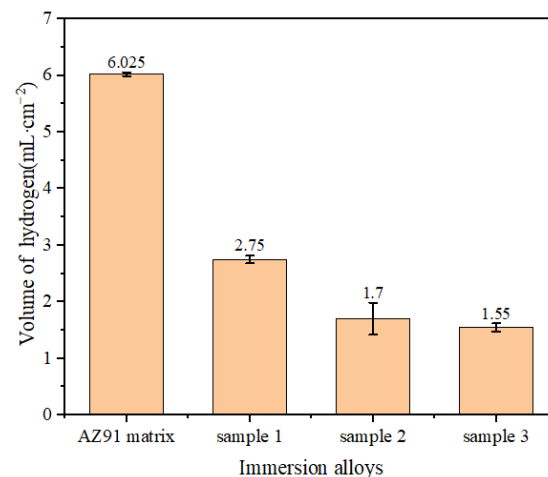


Figure 3. Total hydrogen evolution of samples immersed for 12 h.

As shown in Figure 4, the rate of hydrogen evolution for samples 1, 2 and 3 was lower and their corrosion resistance was higher compared with the AZ91 matrix. The hydrogen evolution rates for the samples tended to level off. The rates for samples 2 and 3 followed similar trajectories to a certain extent, but ultimately, the rate of hydrogen evolution for sample 3 was lower.

From the morphologies of the TiO₂ coating, AZ91 matrix and samples 1, 2 and 3 and from the total amount and rate of hydrogen evolution at the end of the hydrogen evolution experiment, it is apparent that the alloy was corroded by Cl⁻ ions in the experiment. The surface of the AZ91 matrix alloy without any protective coating was exposed to the solution and in direct contact with Cl⁻ ions, and thus, it underwent a strong corrosion reaction, resulting in numerous corrosion pits and many corrosion products being formed on the surface [20]. In comparison, the TiO₂ coating on the surface of sample 1 covered the surface of the AZ91 matrix alloy more completely, and corrosion was confined to the cracks on the coating, namely, to the exposed parts of the AZ91 matrix, and the corrosion reaction was much less severe. In sample 2, since the number of coatings was larger compared with sample 1, the outermost coating layer was more severely cracked, since its adhesion to the base coating was not strong. However, the larger overall thickness of the coating

on sample 2 compared with the coating thickness on sample 1, and the integrity of the substrate coating led to the corrosion of sample 2 being less; in other words, the corrosion resistance was higher. The thickness of the coating on sample 3 was greater than that on sample 2, and the integrity of the outermost coating was also higher. Consequently, the extent of cracking of the coating was smaller, and the coating was fine and uniform. Since only a small part of sample 3's surface was not covered by the TiO₂ coating, the sample showed the best corrosion resistance and the least amount of hydrogen evolution among the four samples [21,22].

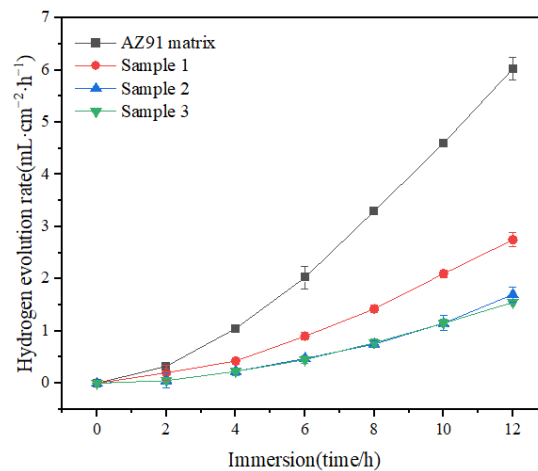


Figure 4. Hydrogen evolution rates for 12 h of immersion.

As shown in Figure 5a, the curve for the AZ91 matrix contained two capacitive arcs with small radii, and a small portion of the inductive arc was in the low-frequency region, indicating that part of the matrix surface was corroded [23]. The curves of samples 1, 2 and 3 had only one capacitive arc segment, and its radius was greater than that in the case of the AZ91 matrix. The corrosion mechanism of the AZ91 matrix was different from that of samples 1, 2 and 3, and the TiO₂ coating caused the corrosion mechanism of the samples to differ. The TiO₂ coating increased the resistance of the AZ91 substrate and effectively enhanced its corrosion resistance. Sample 3 had the best corrosion resistance [24].

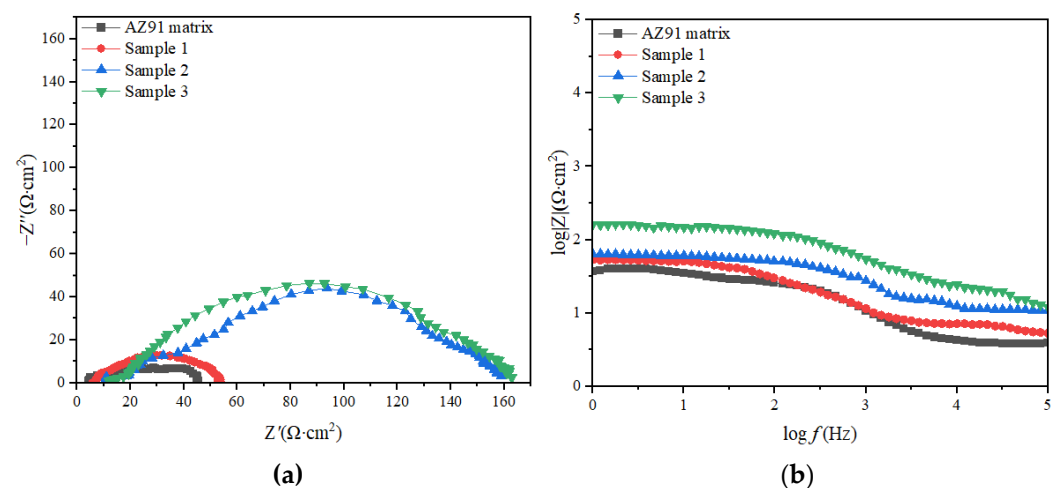


Figure 5. Impedance curves and Bode plots of samples (a) Impedance curves; (b) Bode plots.

In Figure 5b, it is evident that the higher the impedance modulus in the low-frequency region of the material, the higher the material's corrosion resistance [25,26]. The impedance moduli of the AZ91 substrate and samples 1, 2 and 3 were 41.75, 53.73, 158.30 and 162.90 Ω, respectively.

In electrochemical experiments performed to compare the corrosion resistance of magnesium alloys, either the corrosion potential or the corrosion current density of the alloys is compared. The smaller the corrosion current density of a material, the higher its corrosion resistance. When the materials being compared have similar corrosion current densities, the higher the corrosion potential of a material, the higher its corrosion resistance [27].

The corrosion potential and corrosion current density of the AZ91 matrix and samples 1, 2 and 3 are presented in Table 2 (This data is obtained from Figure 6). Compared with the AZ91 matrix, the corrosion potentials of samples 1, 2 and 3 were higher by 100, 330 and 340 mV, respectively, and the corrosion current densities of these samples were lower by 55.4%, 89.8% and 91.7%, respectively [28]. Thus, samples 1, 2 and 3 had higher corrosion resistance than the AZ91 matrix, with sample 3 having the best corrosion resistance and sample 2 having the next best corrosion resistance.

Table 2. Corrosion potential and current density of specimens.

Test Samples	Parameters	E_{corr}/V	$i_{\text{corr}}/\text{A}\cdot\text{cm}^{-2}$
AZ91 matrix		−1.74	8.3×10^{-3}
Sample 1		−1.64	3.7×10^{-3}
Sample 2		−1.41	8.5×10^{-4}
Sample 3		−1.40	6.9×10^{-4}

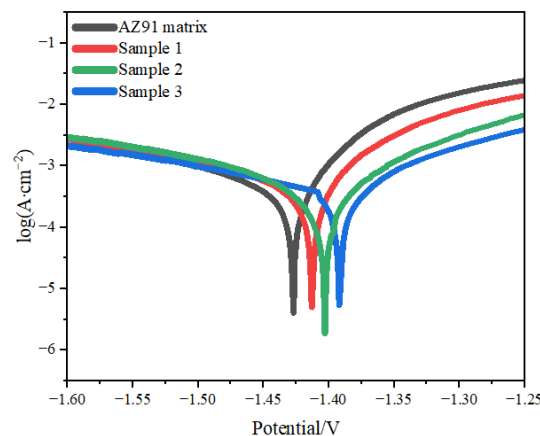


Figure 6. Polarization curves of samples.

It should be noted that for the substrate AZ91 magnesium alloy, the corrosive medium enters the inner chemical transformation film through the TiO_2 coating and the substrate is susceptible to the risk of filiform corrosion. At this time, the corrosion resistance of the system is affected by two factors, one is the porosity of the outer TiO_2 coating and the size of the pores, where the smaller the pore size, the lower the porosity and the lower the possibility of the medium entering the inner layer, and the corrosion behaviour of the system shows the corrosion characteristics of the outer TiO_2 coating [29]. The second is the degree of denseness and thickness of the inner magnesium alloy phosphate film. The higher the density and the greater the thickness, the stronger the impediment to the transfer of corrosion media and corrosion products in it and the lower the likelihood of the corrosion of the AZ91 magnesium alloy [30].

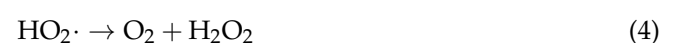
The TiO_2 coating on the AZ91 matrix had stable chemical properties and good corrosion resistance, and it reduced the contact area between the 3.5% NaCl solution and the AZ91 matrix, which retarded the rate of the corrosion reaction, increased the corrosion potential and reduced the corrosion current density of the AZ91 matrix [31]. Sample 3 had the highest corrosion potential and the lowest corrosion current density.

Semiconductor materials generate conduction band electrons and valence band holes by absorbing external radiation and light energy excitation. Those electrons and holes un-

dergo a series of chemical reactions with substances adsorbed on the surface of the catalyst to produce active groups. The photocatalytic mechanism of TiO₂ can be expressed by Equations (1)–(6). Theoretically, as long as the light energy absorbed by the semiconductor ($h\nu$) is not less than its forbidden band width, the electron (e^-) on the valence band can be excited to leap to the conduction band, producing the corresponding hole (h^+) on the valence band, and then h^+ and e^- interact with H₂O, O₂, etc., adsorbed on the surface of TiO₂ to produce $\cdot\text{OH}$, $\cdot\text{O}_2^-$ and other highly reactive groups. There is also the possibility of compounding electrons. The ability of TiO₂ to undergo redox reactions under light conditions is due to its electronic structure characterised by a full valence band and an empty conduction band [32]. When the photon energy reaches or exceeds its band gap energy, the electron can be excited from the valence band to the conduction band, while the corresponding hole is generated in the valence band, that is, the generation of electron, hole pairs. When a suitable trapping agent is present, the recombination of electrons and holes is inhibited and a redox reaction takes place on the surface. Valence band holes are good oxidising agents and conduction band electrons are good reducing agents. Electrons generally react with surface-adsorbed oxygen molecules, while holes react with surface-adsorbed H₂O or OH⁻ ions to form hydroxyl groups with strong oxidising properties [33].

TiO₂ is excited by light to produce h^+ and e^- , a phenomenon that also occurs in ordinary TiO₂, but due to the small particle size of nano-TiO₂, the migration time of h^+ and e^- from the interior of the crystal to the surface is greatly reduced, thus reducing the chance of h^+ and e^- compounding, and thus providing unparalleled photocatalytic activity of ordinary TiO₂. Sometimes, in order to further increase the photocatalytic activity and reduce the chance of compounding photogenerated holes and electrons, additional strong oxidizing or reducing agents are added to the system, which can effectively trap electrons or holes, thus achieving the effective separation of holes and electrons [34].

Light generated by the active group can cause the disintegration of the organic pollutants adsorbed on the surface, and thus, in the presence of light, TiO₂ films have a surface cleaning effect. Upon coming in contact with organic pollutants in the liquid phase, the films can break down the pollutants. Thus, TiO₂ can be used for water purification. Connecting TiO₂ to an external circuit results in a photocurrent passing through it; this is the basis of a solar cell. The anti-corrosion effect of TiO₂ coatings on metals partly results from the semiconductor characteristics of the coatings; the basic principle is shown in Figure 7. In addition, if TiO₂ is in contact with a metal, electrons are injected from the semiconductor to the metal via the conduction band; as a result, the potential of the metal can be shifted in the negative direction to the flatland potential of TiO₂ [35]. The metal is therefore more resistant to corrosion. A water decomposition reaction occurs on the TiO₂ coating [36]. Notably, TiO₂ can be used as a permanent protective coating [37]. Thus, a TiO₂ coating can effectively prevent the corrosion of the AZ91 magnesium alloy.



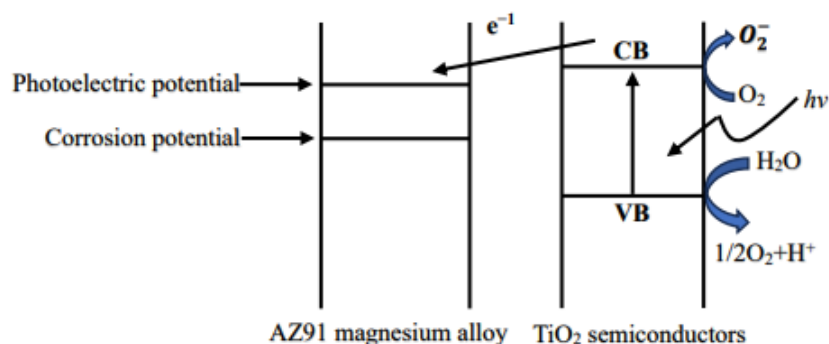


Figure 7. Schematic diagram of the principle of corrosion protection by TiO₂ coating.

4. Conclusions

In this paper, a TiO₂ coating was prepared via the sol-gel method and applied to an AZ91 magnesium alloy matrix. The corrosion resistance was studied and analysed through hydrogen evolution and electrochemical experiments, and the following conclusions were drawn regarding the corrosion resistance based on XRD analysis and SEM:

- (1) The XRD results demonstrate that TiO₂ prepared via the sol-gel method is attached to the surface of AZ91 magnesium alloys after being held at 300 °C for 2 h. SEM analysis reveals that the number of cracks increases after one coating is applied. After three coatings, larger cracks appear or even peel off due to poor adhesion. After five coatings, many stacks appear, and the cracks markedly decrease. Notably, a relatively uniform and stable TiO₂ coating can be formed.
- (2) The hydrogen evolution rates for sample 2 and sample 3 were the slowest and somewhat similar for the 3.5% NaCl solution. However, the final coating of sample 3 was less than that of sample 2, and the total hydrogen evolution of the five layers was the least.
- (3) The corrosion potential of the AZ91 magnesium alloy coated with one, three and five layers of TiO₂ increased by 100 mV, 330 mV and 340 mV, respectively, compared to the base, and the corrosion current density decreased by 55.4%, 89.8% and 91.7%, respectively. The AZ91 substrate has an impedance modulus of 41.75 Ω, whereas those coated with one, three and five layers have impedance moduli of 53.73 Ω, 158.30 Ω and 162.90 Ω, respectively. The impedance modulus, corrosion potential and corrosion current density reveal that the samples coated with five layers have the best corrosion resistance.
- (4) A comprehensive analysis of the hydrogen evolution corrosion rate, total hydrogen evolution, impedance modulus, corrosion potential and corrosion current density of the AZ91 magnesium alloy coated with one, three and five layers of TiO₂ coating reveals that five TiO₂ coatings can significantly improve the corrosion resistance of the AZ91 magnesium alloy surface.

Author Contributions: Conceptualization, G.H. and Y.W. (Yu Wang); software, S.D. and Y.W.; investigation: S.D., G.Z. and Y.W. (Yongyong Wang); validation, D.W.; formal analysis, D.W.; resources, F.Y.; data curation, G.Z., G.H., F.Y. and Y.W. (Yu Wang); writing—original draft, H.T.; writing—review and editing, H.T. and Y.S. All authors have read and agreed to the published version of the manuscript.

Funding: This work was financially supported by the National Natural Science Foundation of China (51665012) and supported by Jiangxi Province Science Foundation for Outstanding Scholarship (20171BCB23061).

Data Availability Statement: No new data were created or analyzed in this study. Data sharing is not applicable to this article.

Conflicts of Interest: The authors declare no conflict of interest.

References

1. Xi, B.; Fang, G.; Xu, S. Multiscale mechanical behavior and micro structure evolution of extruded magnesium alloy sheets: Experimental and crystal plasticity analysis. *Mater. Charact.* **2018**, *135*, 115–123. [[CrossRef](#)]
2. Jia, C.Y.; Huo, Y.M.; He, T.; Yang, W.B.; Huo, C.L.; Liu, K.R. Current status of research on the development of magnesium alloy from process to application. *Agric. Equip. Veh. Eng.* **2022**, *60*, 61–65.
3. Liu, J.A.; Xu, H. The application of magnesium alloy materials and the development of their processing technology. *Light Alloy Process. Technol.* **2007**, *35*, 1–5+54.
4. Upadhyay, G.; Saxena, K.K.; Sehgal, S.; Mohammed, K.A.; Prakash, C.; Dixit, S.; Buddhi, D. Development of Carbon Nanotube (CNT)-Reinforced Mg Alloys: Fabrication Routes and Mechanical Properties. *Metals* **2022**, *12*, 1392. [[CrossRef](#)]
5. Neeraj, S.; Gurpreet, S.; Pardeep, S.; Singla, A. Development of Mg-Alloy by Powder Metallurgy Method and Its Characterization. *Powder Metall. Met. Ceram.* **2019**, *58*, 163–169.
6. Huang, Y.D.; Jiang, B. Editorial for special issue on developments of magnesium alloys for structural and functional applications. *Int. J. Miner. Metall. Mater.* **2022**, *29*, 1307–1309. [[CrossRef](#)]
7. Esmaily, M.; Svensson, J.E.; Fajardo, S.; Biribilis, N.; Frankel, G.S.; Virtanen, S.; Arrabal, R.; Thomas, S.; Johansson, L.G. Fundamentals and advances in magnesium alloy corrosion. *Prog. Mater. Sci.* **2017**, *89*, 92–193. [[CrossRef](#)]
8. de Oliveira, M.C.L.; Antunes, R.A. Graphene-based coatings for magnesium alloys: Exploring the correlation between coating architecture, deposition methods, corrosion resistance and materials selection. *Corros. Rev.* **2022**, *40*, 427–451. [[CrossRef](#)]
9. Cui, X.L.; Jiang, Z.Y. Preparation of nano TiO₂ films. *Adv. Chem.* **2002**, *14*, 325–331.
10. Daubert, J.S.; Hill, G.T.; Gotsch, H.N.; Gremaud, A.P.; Ovental, J.S.; Williams, P.S.; Oldham, C.J.; Parsons, G.N. Corrosion Protection of Copper Using Al₂O₃, TiO₂, ZnO, HfO₂, and ZrO₂ Atomic Layer Deposition. *ACS Appl. Mater. Interfaces* **2017**, *94*, 4192–4201. [[CrossRef](#)]
11. Lee, M.; Han, S.; Kim, C.; Velumani, S.; Han, A.; Kassiba, A.H.; Castaneda, H. ZrO₂/ZnO/TiO₂ Nanocomposite Coatings on Stainless Steel for Improved Corrosion Resistance, Biocompatibility, and Antimicrobial Activity. *ACS Appl. Mater. Interfaces* **2022**, *14*, 13801–13811. [[CrossRef](#)] [[PubMed](#)]
12. Yao, J.; Chen, H.Y.; Liu, L.L. Preparation of TiO₂ coating on AZ91D magnesium alloy surface by sol-gel method and its corrosion performance. *Therm. Process. Technol.* **2012**, *41*, 123–124+127.
13. Ramezani, M.; Ripin, Z.M.; Pasang, T.; Jiang, C.-P. Surface Engineering of Metals: Techniques, Characterizations and Applications. *Metals* **2023**, *13*, 1299. [[CrossRef](#)]
14. Huang, Z.F.; Yong, Q.W.; Xie, Z.H. Stearic acid modified porous nickel-based coating on magnesium alloy AZ31 for high superhydrophobicity and corrosion resistance. *Corros. Commun.* **2023**, *10*, 38–47. [[CrossRef](#)]
15. Zhang, X.; Zhang, Y.; Lv, Y.; Dong, Z.; Hashimoto, T.; Zhou, X. Enhanced corrosion resistance of AZ31 Mg alloy by one-step formation of PEO/Mg-Al LDH composite coating. *Corros. Commun.* **2022**, *6*, 67–83. [[CrossRef](#)]
16. Wan, D.; Wang, Y.; Dong, S.; Xue, Y.; Han, G.; Yang, F.; Tang, H.; Kang, J.; Zeng, G.; Xu, J. Improving corrosion resistance of high strength Mg-Zn-Y alloy through Ca addition. *Corros. Eng. Sci. Technol.* **2022**, *57*, 789–795. [[CrossRef](#)]
17. Zhang, Y.; Zhang, C.L.; Meng, X.; Cao, G.Q.; Li, C.S. Corrosion Protection of Mg Alloy by a TiO₂ Coating Prepared by Sol-Gel Method. *Adv. Mater. Res.* **2013**, *740*, 473–477. [[CrossRef](#)]
18. Shen, G.X.; Chen, Y.; Lin, L.; Lin, C.; Scantlebury, D. Study on a hydrophobic nano-TiO₂ coating and its properties for corrosion protection of metals. *Electrochim. Acta* **2005**, *50*, 5083–5089. [[CrossRef](#)]
19. Pour, F.H.; Behpour, M.; Shabani-Nooshabadi, M.; Jafari, Y. Investigation of corrosion protection properties of TiO₂-CdO nanocomposite coating prepared by sol-gel method on copper. *J. Nanostruct.* **2020**, *10*, 52–63.
20. Zhao, Y.-C.; Zhao, M.-C.; Xu, R.; Liu, L.; Tao, J.-X.; Gao, C.; Shuai, C.; Atrens, A. Formation and characteristic corrosion behavior of alternately lamellar arranged α and β in as-cast AZ91 Mg alloy. *J. Alloys Compd.* **2019**, *770*, 549–558. [[CrossRef](#)]
21. Okouchi, H.; Seki, Y.; Sekigawa, T.; Hira, H.; Kawamura, Y. Nanocrystalline LPSO Mg-Zn-Y-Al Alloys with High Mechanical Strength and Corrosion Resistance. *Mater. Sci. Forum* **2010**, *638–642*, 1476–1481. [[CrossRef](#)]
22. Kavimani, V.; Prakash, K.S.; Gunashri, R.; Sathish, P. Corrosion protection behaviour of r-GO/TiO₂ hybrid composite coating on Magnesium substrate in 3.5 wt.% NaCl. *Prog. Org. Coat.* **2018**, *125*, 358–364. [[CrossRef](#)]
23. Cheng, P.; Zhao, Y.H.; Lu, R.P.; Hou, H. Effect of the morphology of long-period stacking ordered phase on mechanical properties and corrosion behavior of cast Mg-Zn-Y-Ti alloy. *J. Alloys Compd.* **2018**, *764*, 226–238. [[CrossRef](#)]
24. Ashraf, M.A.; Liu, Z.; Peng, W.-X.; Yooysefi, N. Amino acid and TiO₂ nanoparticles mixture inserted into sol-gel coatings: An efficient corrosion protection system for AZ91 magnesium alloy. *Prog. Org. Coat.* **2019**, *136*, 105296. [[CrossRef](#)]
25. Jin, K.; Zhang, Y.Q.; Zhang, T.; Guo, J. Electrochemical corrosion behavior of laser-fused Al-Ti-Ni/C coating on AZ91D magnesium alloy surface. *Electr. Weld. Mach.* **2019**, *49*, 83–87.
26. Liu, P.; Wang, J.M.; Yu, X.T.; Chen, X.-B.; Li, S.-Q.; Chen, D.-C.; Guan, S.-K.; Zeng, R.-C.; Cui, L.-Y. Corrosion resistance of bioinspired DNA-induced Ca-P coating on biodegradable magnesium alloy. *J. Magnes. Alloys* **2019**, *7*, 144–154. [[CrossRef](#)]
27. Wang, X.R. *Preparation and Performance Study of Superhydrophobic Coatings on Titanium Alloy*; Huazhong University of Science and Technology: Wuhan, China, 2019.
28. Wang, D.; Zhang, J.; Xu, J.; Zhao, Z.; Cheng, W.; Xu, C. Microstructure and corrosion behavior of Mg-Zn-Y-Al alloys with long-period stacking ordered structures. *J. Magnes. Alloys* **2014**, *2*, 78–84. [[CrossRef](#)]

29. Rivero, P.J.; Maeztu, J.D.; Berlanga, C.; Miguel, A.; Palacio, J.F.; Rodriguez, R. Hydrophobic and Corrosion Behavior of Sol-Gel Hybrid Coatings Based on the Combination of TiO₂ NPs and Fluorinated Chains for Aluminum Alloys Protection. *Metals* **2018**, *8*, 1076. [[CrossRef](#)]
30. Jiang, P. *Research on Composite Coatings Prepared by Chemical Transformation and Sol-Gel Technology on the Surface of AZ91D Magnesium Alloy*; Harbin Engineering University: Harbin, China, 2008.
31. Wang, S.X.; Ma, X.H.; Bai, J.T.; Du, T.; Ma, R.; Du, A.; Zhao, X.; Fan, Y.; Li, G. Study of the corrosion behavior and mechanism of a hot-dipping Zn–6Al–3Mg alloy coating in 3.5 wt% neutral NaCl solution. *Surf. Coat. Technol.* **2023**, *464*, 129576. [[CrossRef](#)]
32. Shao, J.; Wang, X.-T.; Xu, H.; Zhao, X.-D.; Niu, J.-M.; Zhang, Z.-D.; Huang, Y.-L.; Duan, J.-Z. Photoelectrochemical Performance of SnS₂ Sensitized TiO₂ Nanotube for Protection of 304 Stainless Steel. *J. Electrochem. Soc.* **2021**, *168*, 016511. [[CrossRef](#)]
33. Yu, X.Y.; Cheng, J.J.; Du, Y.J. Titanium dioxide photocatalytic materials. *Chem. World* **2000**, *11*, 567–570.
34. Fan, C.Z.; Xiao, J.P.; Ding, Y.W. Progress in the preparation and photocatalytic reaction of TiO₂ nanoparticles. *Sci. Bull.* **2001**, *46*, 265–273.
35. Ohko, Y.; Saitoh, S.; Tatsuma, T.; Fujishima, A. Photoelectrochemical Anticorrosion and Self-Cleaning Effects of a TiO₂ Coating for Type 304 Stainless Steel. *J. Electrochem. Soc.* **2001**, *148*, B24–B28. [[CrossRef](#)]
36. Lu, G.; Sun, M.; Chen, Z.; Jiang, X.; Jing, J. Efficient TiO₂/AgInS₂/ZnS Nanoarchitecture Photoelectrode for the Photoelectrochemical Cathodic Protection of Copper in NaCl Solution. *J. Electrochem. Soc.* **2020**, *167*, 141505. [[CrossRef](#)]
37. Sinulingga, K.; Sirait, M.; Marpaung, T.M. Effect of Temperature Variation Characteristics Of Crystal Structure and Morphology of Nano TiO₂ Coating On Metal Anti-Corrosion Coating by Sol-Gel Method Spin Coating. *J. Phys. Conf. Ser.* **2020**, 1485. [[CrossRef](#)]

Disclaimer/Publisher’s Note: The statements, opinions and data contained in all publications are solely those of the individual author(s) and contributor(s) and not of MDPI and/or the editor(s). MDPI and/or the editor(s) disclaim responsibility for any injury to people or property resulting from any ideas, methods, instructions or products referred to in the content.